Original Article

A pilot study of highly accelerated 3D MRI in the head and neck position verification for MR-guided radiotherapy

Yihang Zhou, Oi Lei Wong, Kin Yin Cheung, Siu Ki Yu, Jing Yuan

Medical Physics and Research Department, Hong Kong Sanatorium & Hospital, Hong Kong, China

Correspondence to: Yihang Zhou, PhD. Medical Physics and Research Department, Hong Kong Sanatorium & Hospital, 11/F, HKSH Eastern Medical Center, 5 A Kung Ngam Village Road, Shau Kei Wan, Hong Kong, China. Email: yihang.zhou@outlook.com.

Background: To evaluate the performance of a highly accelerated 3D MRI on inter-fractional positional measurement for MR-guided radiotherapy (MRgRT) in the head and neck (HN).

Methods: Fourteen healthy volunteers received 159 scans on a 1.5 T MR-sim to simulate MRgRT fractions. MRI acquisition included a high-resolution (HQI-MRI, voxel-size =1.05×1.05×1.05 mm^3, duration =5 min) and a highly-accelerated low-resolution (true-LQI-MRI, acceleration-factor =9, voxel-size =1.4×1.4×1.4 mm^3, duration =86 s) T1w spin-echo sequence (TR/TE =420/7.2 ms). The first session HQI-MRI was used as the reference to mimic planning MRI. Other HQI-MRI was also retrospectively down-sampled in K-space and GRAPPA reconstructed to generate pseudo-LQI-MRI. Inter-sessional positional shift calculated from HQI-MRI, true-LQI-MRI and pseudo-LQI-MRI rigidly registering to the reference were analyzed and compared in the overall HN and the sub-regions of brain, nasopharynx, oropharynx and hypopharynx.

Results: The calculated SD of systematic errors (Σ) from HQI-MRI/pseudo-LQI-MRI/true-LQI-MRI images for overall HN were 1.11/1.14/1.08, 0.28/0.26/0.29, 0.43/0.44/0.60, and 0.77/0.79/0.74 mm for translation in LR, AP, SI and 3D, respectively; The corresponding RMS of random errors (σ) were 0.97/0.98/0.96, 0.28/0.27/0.26, 0.77/0.77/0.72, and 0.85/0.87/0.85 mm. For all sub-regions, brain showed the smallest Σ and σ in 3D. Other sub-regions showed direction-dependent error patterns, but the positioning results were consistent, independent of the datasets used for registration.

Conclusions: A highly-accelerated 3D-MRI could be used for MR-guided HN radiotherapy without compromising position verification accuracy.

Keywords: Image-guided-radiotherapy (IGRT); MR-guided radiotherapy (MRgRT); position verification; image registration; systematic error; random error

Submitted Apr 24, 2019. Accepted for publication Jun 16, 2019.
doi: 10.21037/qims.2019.06.18
View this article at: http://dx.doi.org/10.21037/qims.2019.06.18

Introduction

Imaging-guided radiotherapy (IGRT) has been greatly reshaped the conventional radiotherapy (RT) practice and improved RT treatment outcomes evidenced by many clinical trials (1,2). Among the complicated processes of IGRT workflow, patient position verification via imaging is a crucial step for the precise treatment delivery, in particular for the fractionized RT treatment schemes, because there are still considerable subject- and tissue-dependent position uncertainties in multiple fractions even with the use of immobilization devices, internal and/or external fiducials and external positioning laser for alignment (3,4). Many modern radiotherapy treatment machines have been equipped with on-board imaging units for position verification purpose, most of which are X-ray based, such as plain or orthogonal X-ray, cone beam computerized tomography (CBCT) and megavolts CT (MVCT) (5).

These X-ray based on-board imaging units, although very useful, are associated with the limitations of ionizing radiation, and relatively poor image quality, and sometimes long acquisition time (5-9). In recent years, MR-guided radiotherapy (MRgRT) has been proposed, developed, and is translating into a clinical tool by taking the advantages of non-ionizing radiation feature, superior soft tissue contracts and functional imaging capability of MRI (10-17). In the workflow of MRgRT, MRI-based positional verification is anticipated to further reduce the position uncertainty owing to its superior soft tissue contrasts and arbitrary image plane acquisition (18-21).

MRI-based position verification could be implemented in two ways, either on-line or off-line with the treatment machine. The on-line MRI position verification can only be implemented on the recent introduced hybrid MR-guided radiotherapy (MRgRT) modalities, such as MR-LINAC (19,22) and MR-Cobalt 60 radiotherapy machine (23), where on-board positioning MR images can be obtained in a patient on the treatment machine prior to beam-on. In comparison, the off-line MRI position verification acquires the MR images of a patient with the identical treatment position on a dedicated MR scanner, called MR-simulator (MR-sim), equipped with RT-standard 3D positioning laser and compatible with immobilization devices. Immediately after the MRI-sim scan, the patient in his/her setup position is transferred to the RT treatment machine via a trolley- or shuttle-based transfer system in a short time to minimize the risk of patient positional change. Meanwhile, the acquired MR images are also transferred to the treatment machine to be co-registered with the planning images for position verification and correction prior to radiation dose delivery (18,24).

The requirement for MRI on position verification of MRgRT is much different from the use of MRI for radiotherapy treatment planning. For treatment planning, the major purpose and advantage of MRI is to better define the treatment targets as well as the organs-at-risk (OARs) by taking the advantage of supreme MRI soft tissue contrast over CT (25,26). Therefore, high MR image quality in terms of spatial resolution, signal-to-noise ratio (SNR), contrast-to-noise ratio (CNR), geometric fidelity and artifact is critically demanded, so has to be obtained at the cost of long MRI scan time. For MRI position verification, the requirements on superior MRI quality is much less critical as long as the positional shift calculated by registering the positioning MRI to planning image is not much deviated from the ground truth. However, on the other hand, fast MRI acquisition with a short scan time, either implemented on-line or off-line, becomes crucial and highly desirable for minimizing the possible positional change and maximizing the patient comfort and workflow efficiency.

It is well acknowledged that MR image quality, e.g., spatial resolution and image artifact, could considerably deteriorate with shorter scan time. As such, a critical concern on the accuracy and reliability of position verification using fast MRI is that compromised imaging quality might significantly affect the image co-registration accuracy, and thus affect the decision and action on positional correction. As such, the major purpose of this pilot study is two-fold. We aim to rigorously and quantitatively assess the influence of image quality reduction associated with a fast MRI scan on the position verification accuracy in the head and neck in a simulated fractionized RT setting using a dedicated 1.5 T MR-simulator. In addition, we attempt to implement such a fast MRI acquisition and evaluate it for MR-based position verification, preferably shorter than 90 seconds, on the 1.5 T MRI-simulator.

Methods

A total of 14 healthy volunteers, aged between 24 and 40 years, were prospectively recruited for this ethics approved study. Informed consent was obtained from each subject.

Scan setup and data acquisition

All MR scans were conducted with a 1.5-Tesla MR-simulator (MAGNETOM Aera, Siemens Healthineers, Erlangen, Germany) on which the patient table was overlaid with a flat couch-top (Diacor, Salt Lake City, Utah, USA). A customized head-and-neck and shoulder thermoplastic mask (Orfit Industries, Belgium), and a standard neck rest were used for immobilization. This scan position was identical to the head and neck RT treatment position in our hospital. Permanent lines were drawn on the thermoplastic mask, and MRI visible fiducial markers (PinPoint, Beekley Medical, USA) were attached at the cross points of the drawn lines. Subjects were positioned by aligning the drawn lines on the mask with a well-calibrated 3-dimensional positioning laser (DORADOnova MR3T, LAP GmbH Laser Applikationen, Luneburg, Germany). Two 4-channel surface coils were wrapped around the head using two bi-lateral coil holders (Orfit Industries, Belgium). An 18-channel flexible body coil was anteriorly positioned on the subject. The embedded spine coil array underneath the flat couch-top was used to

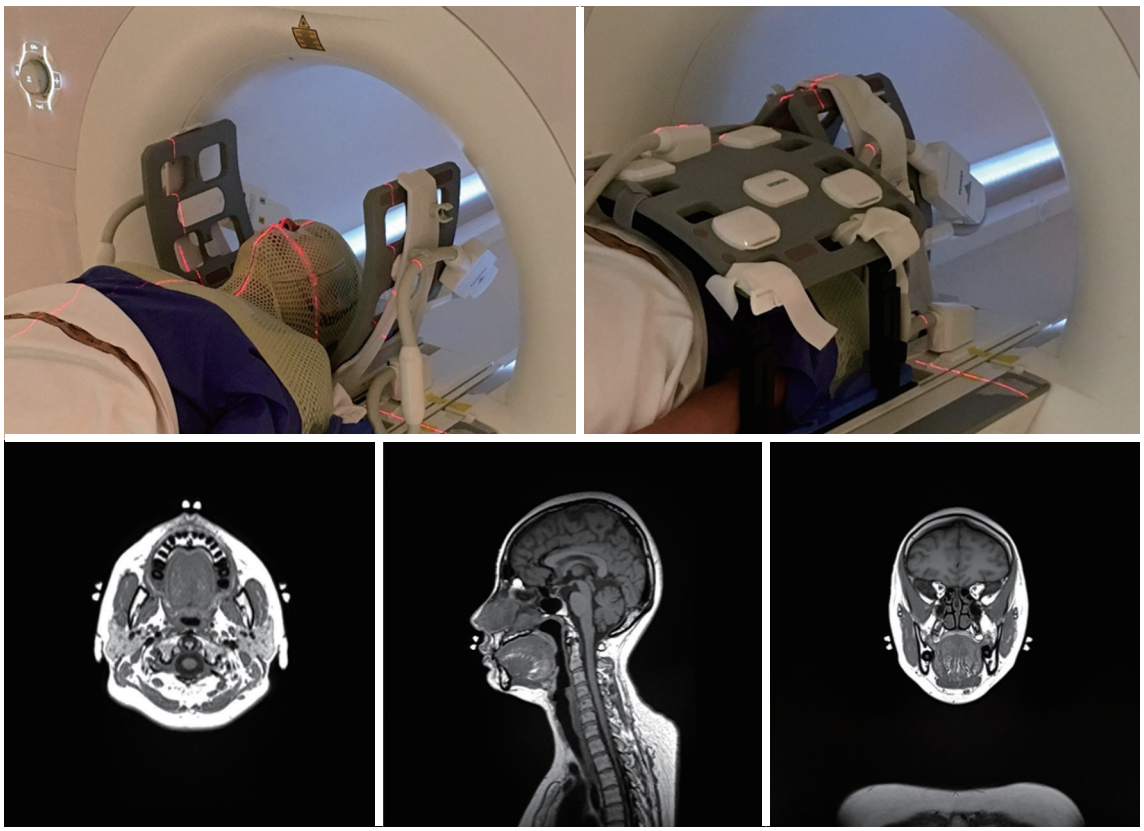

Figure 1 Top: Illustration of a typical volunteer setup that was immobilized and aligned with the positioning laser system; Bottom: One representative slice of the acquired high-resolution MR image in the axial, sagittal and coronal plane.

cover the posterior neck and chest for acquisition. All coils did not directly touch the patient body. A typical volunteer setup that was immobilized and aligned with the positioning laser system is illustrated in *Figure 1*.

All subjects were each time positioned, aligned and underwent a number of scans on the MR-sim to simulate the multiple fractions in the HNC RT treatment. The subjects No. 1–3 underwent 40, 38 and 32 scans, respectively, within 1 month; subjects No. 4–5 underwent 6 and 7 scans, respectively, within 1 week, and the remaining nine subjects No. 6–14 received 4 scans within 1 day, yielding a total imaging fractions of 159 in all subjects. All MRI scans in each subject included a high quality imaging (HQI) protocol with a T1-weighted 3D-SPACE (Sampling Perfection with Application optimized Contrasts using different flip angle Evolution) sequence accelerated with GRAPPA (GeneRalized Auto-calibrating Partially Parallel Acquisitions) technique (27). The imaging parameters were FOV =470 mm (LR, phase-encoding direction) ×470 mm (SI, frequency-encoding direction) ×269 mm (AP, slice-encoding direction), matrix size =448 (LR) ×448 (SI) ×256 (AP), isotropic voxel size =1.05×1.05×1.05 mm^3; TR/TE =420/7.2 ms, echo train length (ETL) =40, GRAPPA-acceleration-factor =3(AP), slice-encoding partial Fourier factor =6/8, bandwidth =657 Hz/pixel, acquisition time = 5 min 1 sec.

The subjects No. 1–5 underwent a subsequent low-quality imaging (LQI) acquisition immediately after their HQI acquisition in each scan without re-positioning to maximize the intra-scan position consistency. This LQI acquisition protocol was developed by reducing the spatial-resolution and applying a very high acceleration factor on both phase-encoding and slice-encoding directions in order to achieve a scan time shorter than 90 seconds. TR/TE were kept the same as the HQI protocol without changing the image contrast. The image parameters associated with the LQI protocol were FOV =448 mm (LR, phase-encoding direction) ×448 mm (SI, frequency-encoding direction) ×291 mm (AP, slice-encoding direction), matrix size = 320 (LR) ×320 (SI) ×208 (AP), isotropic voxel size

= 1.40×1.40×1.40 mm^3; TR/TE =420/7.2 ms, ETL =40, GRAPPA factor =9 =3(LR) ×3(AP), slice-encoding partial Fourier factor =5/8, Bandwidth =657 Hz/pixel, acquisition time =86 sec.

For all MRI scans, prescan normalization, a technique to compensate receive-B1 field inhomogeneity on Siemens MRI platform, and console-integrated 3D geometric distortion correction were applied.

Data analysis

All acquired MR data were exported as DICOM images and processed off-line using 3D Slicer version 4.5.0 (http://www.slicer.org) (28).

The MR images acquired using the HQI protocol in the first MRI scan of each subject, named reference-MRI, were used as the positioning reference in the high image quality planning MRI. The MR images acquired by HQI protocol in the following scans, named HQI-MRI, were retrospectively further down-sampled in K-space domain by 4-fold and then reconstructed using GRAPPA reconstruction algorithm in MATLAB (version 2015b, Mathworks, Natick, MA, USA) to generate pseudo-LQI-MRI images. The major purpose of this pseudo-LQI-MRI image generation was to replicate the identical subject positioning to that in the HQI MR images but exacerbate the GRAPPA-related image artifacts to evaluate its influence on image registration accuracy compared to the true fast-scan low-quality MR (true-LQI-MRI) images.

Inter-fractional subject positional variation was quantified by rigidly registering different MRI data sets to reference-MRI using normalized mutual information algorithm. Overall positional variation in the head and neck was firstly calculated by using the entire image volume for registration. After that, sub-regional positional variation was calculated by registering individually on the volumes-of-interest (VOIs) of brain, nasopharynx (from the base of the skull to the upper surface of the soft palate), oropharynx (soft palate to the base of the tongue inferiorly) and hypopharynx (the epiglottis to the division of the esophagus and larynx). The registration transformation matrices were used to calculate the translation in left-right (LR), anterior-posterior (AP) and superior-inferior (SI) directions and the rotation in roll, pitch and yaw directions. Translation to right, anterior and superior direction and rotation to the clock-wise direction was defined as positive.

The rigid registration of HQI-MRI to reference-MRI supposed to have the least registration, so was used as the baseline of inter-fractional positional variation. For comparison, pseudo-LQI-MRI was also rigidly registered to reference-MRI with the identical registration setting. The positional shifts of translation and rotation calculated from this pseudo-LQI-to-reference registration were pair-wisely compared to those from HQI-to-reference registration in the overall head and neck and the sub-regions of brain, nasopharynx, oropharynx and hypopharynx.

In addition, in the subjects No. 1–5 on whom the true-LQI-MRI was acquired, true-LQI-MRI was rigidly registered to reference-MRI. The calculated positional shifts from true-LQI-to-reference registration were compared with those from HQI-to-reference registration for further evaluation.

Statistical method

The agreement of positional shift calculated from HQI-to-reference registration and pseudo-LQI-to-reference registration were analyzed using Bland-Altman plot. To compare the calculated positional shift difference between the HQI-to-reference registration and true-LQI-to-reference registration, only paired student *t*-test was conducted by considering the possible presence of intra-scan subject positional change. A P value of 0.05 or smaller was considered statistically significant.

The group systematic error (M), SD of systematic error (Σ) and root-mean-square (RMS) of random errors (σ) of translation and rotation (29) derived from HQI-to-reference registration, pseudo-LQI-to-reference registration and true-LQI-to-reference registration were calculated and compared between the overall head and neck and the sub-regions.

Results

Translational and rotational displacement

The comparison of positional shifts of translation and rotation calculated from this pseudo-LQI- and HQI-to-reference registration in the overall head and neck and the sub-regions of brain, nasopharynx, oropharynx and hypopharynx was shown in *Table 1*. *Figure 2* showed the boxplot of translational and rotational shift of subject positioning relative to the reference-MRI calculated from HQI- and pseudo-LQI-to-reference registration in the overall head and neck, and the sub-regions of brain, nasopharynx, oropharynx and hypopharynx. Significant differences between HQI- and pseudo-LQI-to-reference

Table 1 The average displacements and standard deviation of translation in LR, SI and AP directions and rotation in roll, pitch and yaw directions calculated from pseudo-LQI- and HQI-to-reference registration in the overall head and neck and the sub-regions of brain, nasopharynx, oropharynx and hypopharynx

Volumes-of-interest	3D translation (mm)						3D rotation (°)					
	LR		AP		SI		Roll		Pitch		Yaw	
	HQI	p-LQI	HQI	p-LQI	HQI	p-LQI	HQI	p-LQI	HQI	p-LQI	HQI	p-LQI
Overall												
Mean	0.10	0.09	−0.20	−0.04	−0.08	0.11	0.05	0.03	0.00	0.00	0.24	0.19
SD	0.96	0.97	0.34	0.33	0.75	0.78	0.15	0.15	0.01	0.01	0.59	0.47
Paired *t*-test to HQI		0.81		0.00		0.00		0.03		0.03		0.04
Brain												
Mean	0.26	0.26	−0.20	0.01	−0.15	−0.06	0.04	0.00	0.00	0.00	0.47	0.46
SD	0.89	0.87	0.70	0.67	0.83	0.78	0.43	0.41	0.01	0.01	1.52	1.50
Paired *t*-test to HQI		0.79		0.00		0.25		0.35		0.23		0.17
Nasopharynx												
Mean	0.24	0.26	−0.24	−0.08	−0.16	−0.16	0.05	0.05	0.00	0.00	0.46	0.45
SD	1.19	1.15	0.89	0.87	0.86	0.85	0.54	0.53	0.01	0.01	1.53	1.51
Paired *t*-test to HQI		0.40		0.00		0.84		0.80		0.31		0.94
Oropharynx												
Mean	0.18	0.18	−0.17	0.00	−0.12	−0.08	0.01	−0.03	0.00	0.00	0.40	0.36
SD	1.16	1.11	0.69	0.65	0.75	0.72	0.48	0.45	0.01	0.01	1.43	1.35
Paired *t*-test to HQI		0.59		0.00		0.07		0.08		0.04		0.35
Hypopharynx												
Mean	0.08	0.03	0.02	0.11	−0.29	−0.21	0.21	0.13	0.00	0.00	0.18	0.13
SD	1.03	0.97	0.72	0.69	0.79	0.79	0.28	0.28	0.01	0.01	1.03	0.96
Paired *t*-test to HQI		0.51		0.02		0.00		0.00		0.89		0.02

registration along AP direction for overall head-and-neck and all sub-regions (P<0.01), and along SI direction for overall and hypopharynx (P<0.01) were observed using paired *t*-test. It is worth noting that the absolute differences in these translational displacements were mostly much below 1 mm level, although significance was reached in the sense of statistics, which would not compromise positioning accuracy and precision much in practice even for precise radiosurgery purpose. *Figure 3* showed the Bland-Altman plot between the difference and the average between the HQI- and pseudo-LQI-to-reference registration of the overall head and neck and the sub-regions. Most measurements were distributed within the acceptable limits of variation, indicating strong registration consistency between pseudo-LQI- n and HQI-to-reference registration.

Table 2 presented the average displacements and standard deviation of translation in LR, SI and AP and rotation in roll, pitch and yaw of for the overall and sub-regions calculated from HQI- and true-LQI-to-reference registration, respectively. *Figure 4* showed the box-plot of group's inter-methodological translation and rotation of overall and sub-regions. Significant translation shift differences were only observed along SI direction in the overall head and neck and oropharynx (P<0.01) using paired *t*-test.

Systematic and random error

The calculated systematic and random errors are

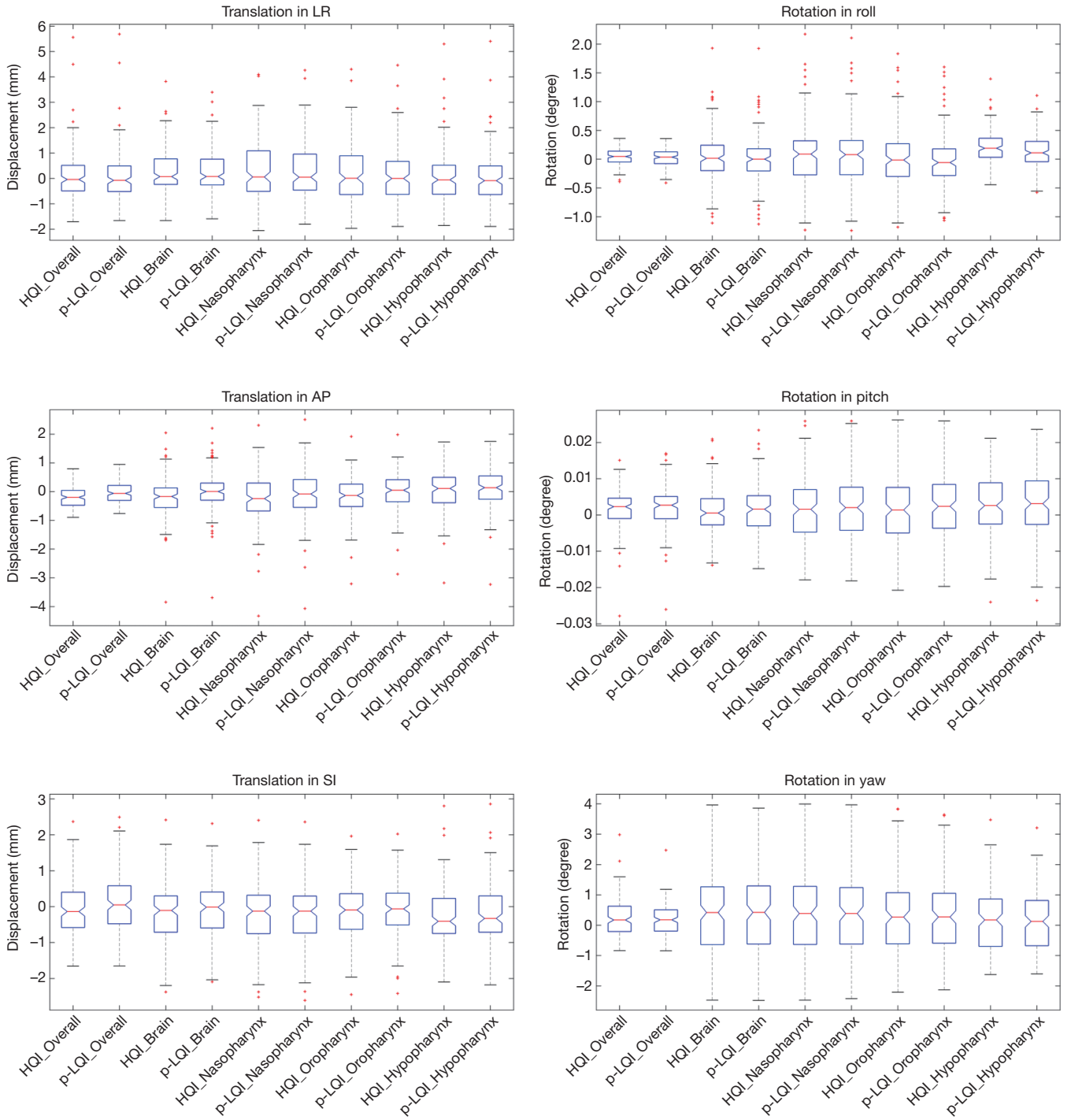

Figure 2 The boxplot of translational and rotational shift of subject positioning relative to the reference-MRI calculated from HQI- and pseudo-LQI-to-reference registration in the overall, and the sub-regions of brain, nasopharynx, oropharynx and hypopharynx.

summarized in *Table 3*. The calculated SD of systematic error (Σ) from HQI/pseudo-LQI/true-LQI images for overall registration was 1.11/1.14/1.08, 0.28/0.26/0.29, 0.43/0.44/0.60, and 0.77/0.79/0.74 mm for translation in LR, AP, SI and 3D, respectively; The RMS of random error (σ) in the corresponding translation direction was

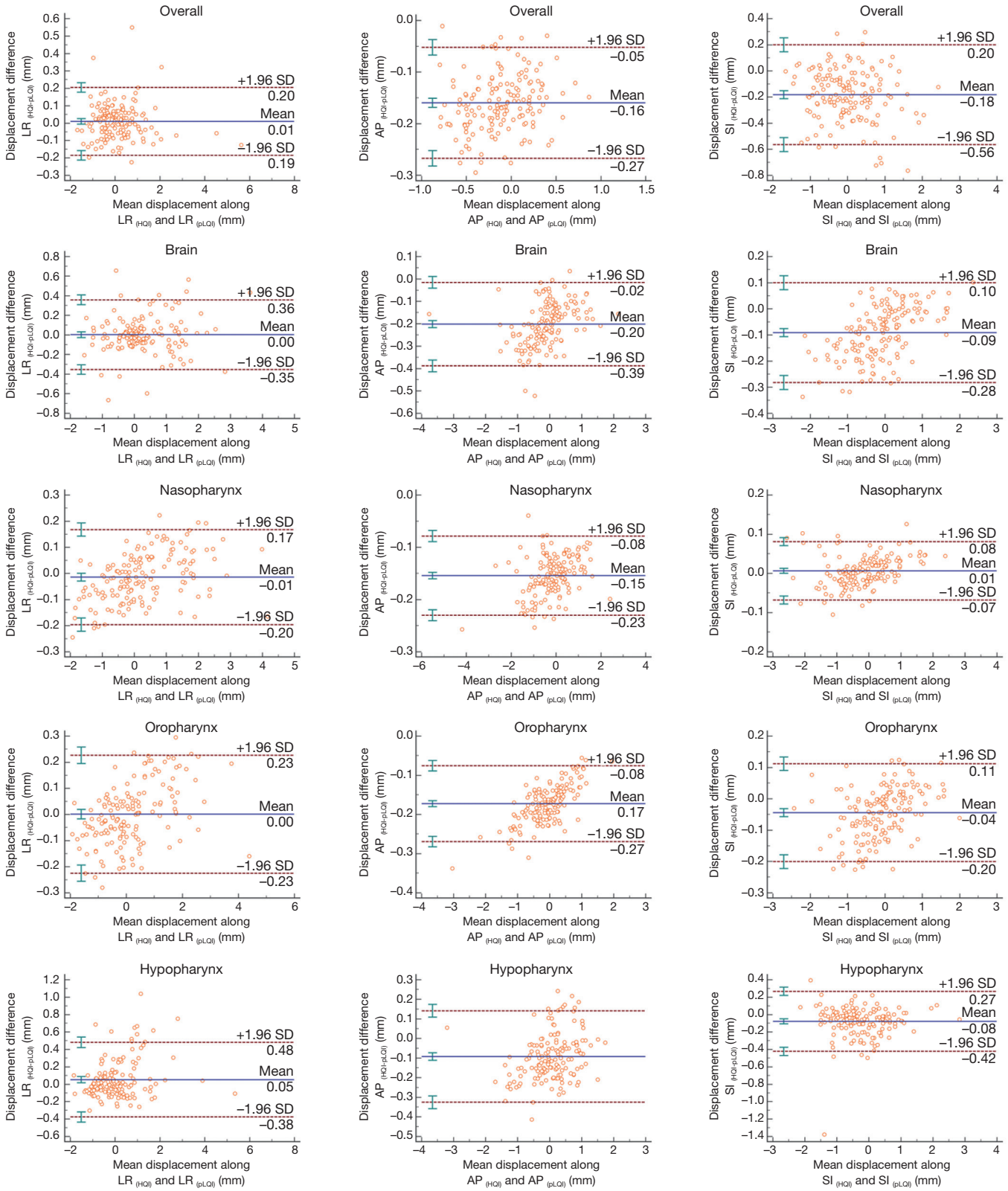

Figure 3 The Bland-Altman plot of the agreement of inter-fractional positional shift calculated from HQI- and pseudo-LQI-to-reference registration.

Table 2 The average displacements and standard deviation of translation in LR, SI and AP directions and rotation in roll, pitch and yaw directions calculated from true-LQI- and HQI-to-reference registration in the overall head and neck and the sub-regions of brain, nasopharynx, oropharynx and hypopharynx

Volumes-of-interest	3D translation (mm)						3D rotation (°)					
	LR		AP		SI		Roll		Pitch		Yaw	
	HQI	t-LQI	HQI	t-LQI	HQI	t-LQI	HQI	t-LQI	HQI	t-LQI	HQI	t-LQI
Overall												
Mean	0.11	0.13	−0.25	−0.27	−0.20	−0.33	0.06	0.08	0.00	0.00	0.26	0.22
SD	1.03	1.01	0.34	0.32	0.70	0.71	0.16	0.17	0.01	0.01	0.63	0.59
Paired *t*-test to HQI		0.63		0.13		0.00		0.01		0.19		0.04
Brain												
Mean	0.19	0.30	−0.27	−0.22	−0.31	−0.30	0.07	0.03	0.00	0.00	0.43	0.50
SD	0.14	0.92	0.68	0.65	0.75	0.82	0.39	0.42	0.01	0.01	1.52	1.62
Paired *t*-test to HQI		0.55		0.71		0.13		0.54		0.18		0.45
Nasopharynx												
Mean	0.25	0.29	−0.30	−0.29	−0.31	−0.40	0.07	0.06	0.00	0.00	0.49	0.47
SD	1.26	1.26	0.90	0.77	0.82	0.82	0.54	0.48	0.01	0.01	1.64	1.63
Paired *t*-test to HQI		0.46		0.69		0.03		0.89		0.29		0.62
Oropharynx												
Mean	0.19	0.21	−0.20	−0.23	−0.26	−0.39	0.00	0.08	0.00	0.00	0.43	0.37
SD	1.23	1.22	0.71	0.58	0.71	0.69	0.50	0.40	0.01	0.01	1.54	1.47
Paired *t*-test to HQI		0.76		0.38		0.00		0.02		0.64		0.19
Hypopharynx												
Mean	0.10	0.06	0.05	−0.01	−0.46	−0.49	0.23	0.25	0.00	0.00	0.20	0.15
SD	1.09	1.07	0.75	0.64	0.68	0.66	0.27	0.24	0.01	0.01	1.09	1.03
Paired *t*-test to HQI		0.43		0.15		0.49		0.53		0.01		0.11

0.97/0.98/0.96, 0.28/0.27/0.26, 0.77/0.77/0.72, and 0.85/0.87/0.85 mm respectively. All these differences were less than 1 mm. For different VOIs, the smallest positional error was found in AP translation and pitch rotation. Comparing across all VOIs, brain tended to have the smallest Σ and σ in 3D for all HQI/pseudo-LQI/true-LQI registration. Other sub-regions showed different error patterns in different directions, and the error results were consistent between all calculations regardless of the datasets used for registration.

Discussion

In this pilot study, we prospectively investigated the feasibility and accuracy of a highly accelerated MRI in the head and neck position verification for MR-guided radiotherapy using a 1.5 T MR-sim on a cohort of healthy volunteers. The results showed that the image quality reduction associated with the highly accelerated fast MRI did not necessarily compromise the image registration accuracy and thus positional shift calculation, so potentially helpful in the MR-based position verification for fractionized head and neck RT.

There are a number of factors should be considered in the design of MR-based positional scan. First, MRI acquisition based on 3D-sequence is preferable over 2D-sequence to obtain isotropic voxel size and smaller geometric distortion in the imaged volume, in particular

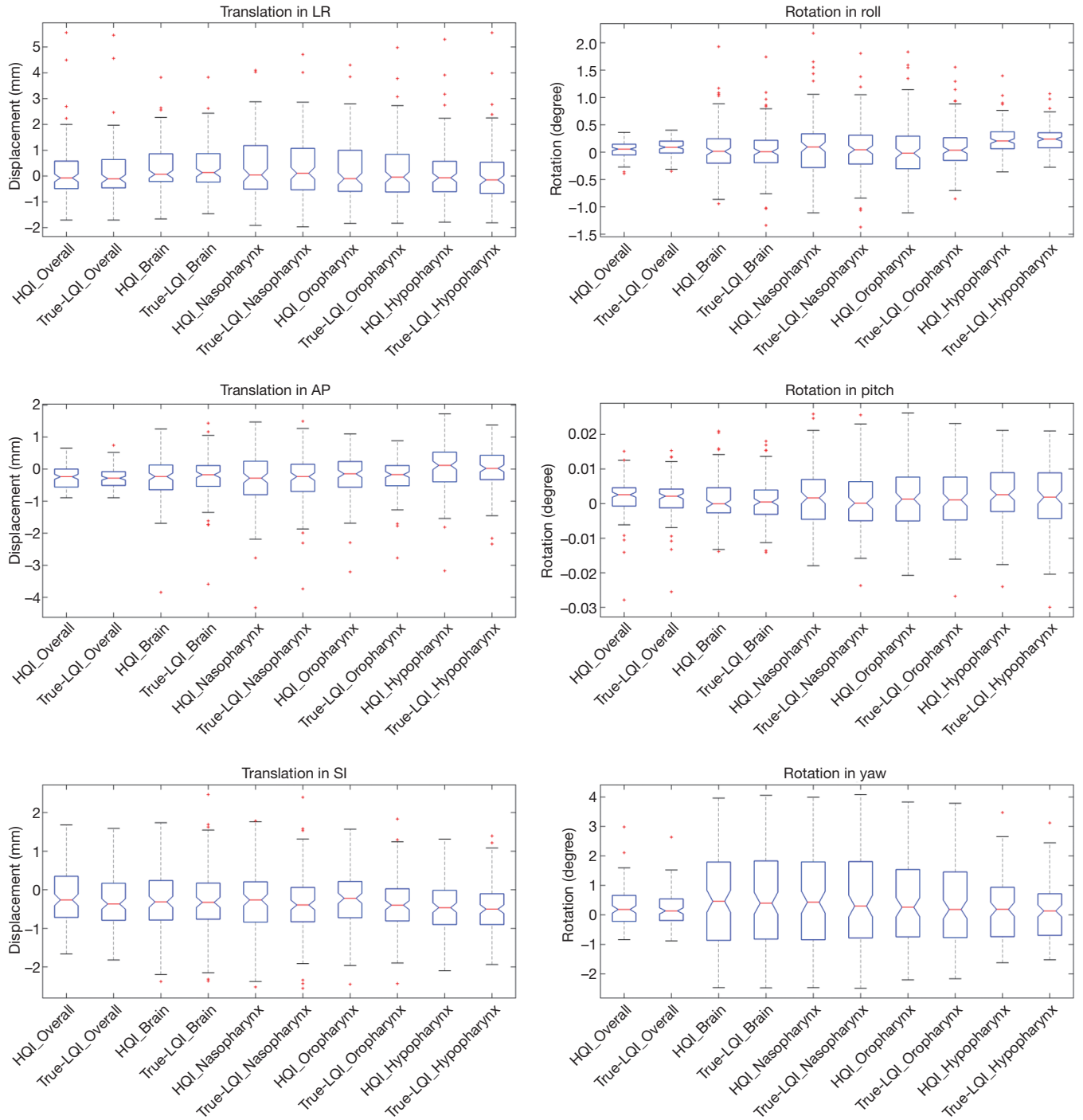

Figure 4 The boxplot of translational and rotational shift of subject positioning relative to the reference-MRI calculated from HQI- and true-LQI-to-reference registration in the overall, and the sub-regions of brain, nasopharynx, oropharynx and hypopharynx.

in the through-plane direction (30). Meanwhile, parallel acceleration could be more efficiently applied on both phase-encoding and slab-encoding directions for scan time reduction. Spin-echo sequence is advantageous over gradient-echo sequence due to its less proneness to B0 inhomogeneities, tissue or implant induced susceptibility

Table 3 The calculated systematic and random errors in 3D translation and rotation relative to the reference-MRI calculated from HQI- and pseudo-LQI-to-reference registration in the overall head and neck, and the sub-regions.

Volumes-of-interest	3D translation												3D rotation											
	LR			AP			SI			3D			Roll			Pitch			Yaw			3D		
	HQI	p-LQI	t-LQI	HQI	p-LQI	t-LQI	HQI	p-LQI	t-LQI	HQI	p-LQI	t-LQI	HQI	p-LQI	t-LQI	HQI	p-LQI	t-LQI	HQI	p-LQI	t-LQI	HQI	p-LQI	t-LQI
Overall																								
Group systematic error M (mm)	0.48	0.47	0.51	−0.13	0.02	−0.14	−0.05	0.16	−0.14	1.33	1.34	1.37	0.00	0.00	0.04	0.00	0.00	0.00	0.11	0.08	0.14	0.47	0.40	0.45
SD of systematic error Σ (mm)	1.11	1.14	1.08	0.28	0.26	0.29	0.43	0.44	0.60	0.77	0.79	0.74	0.16	0.16	0.16	0.00	0.00	0.00	0.50	0.40	0.43	0.28	0.21	0.23
RMS of random error σ (mm)	0.97	0.98	0.96	0.28	0.27	0.26	0.77	0.77	0.72	0.85	0.87	0.85	0.12	0.11	0.11	0.01	0.01	0.01	0.36	0.29	0.37	0.29	0.22	0.30
Brain																								
Group systematic error M (mm)	0.45	0.46	0.49	−0.23	−0.02	−0.18	−0.26	−0.15	−0.18	1.45	1.34	1.45	0.10	0.06	0.06	0.00	0.00	0.00	0.16	0.16	0.22	1.38	1.34	1.35
SD of systematic error Σ (mm)	0.65	0.67	0.65	0.64	0.57	0.46	0.76	0.67	0.85	0.43	0.40	0.45	0.50	0.45	0.40	0.00	0.00	0.00	1.47	1.45	1.43	0.64	0.62	0.61
RMS of random error σ (mm)	0.75	0.74	0.74	0.52	0.52	0.63	0.74	0.71	0.79	0.71	0.74	0.78	0.34	0.33	0.38	0.01	0.00	0.00	0.77	0.75	0.78	0.65	0.65	0.66
Nasopharynx																								
Group systematic error M (mm)	0.54	0.56	0.60	−0.35	−0.21	−0.28	−0.28	−0.30	−0.28	1.84	1.80	1.80	0.14	0.16	0.11	0.00	0.00	0.00	0.16	0.15	0.21	1.46	1.44	1.38
SD of systematic error Σ (mm)	1.02	0.99	1.05	0.91	0.85	0.60	0.83	0.66	0.89	0.70	0.72	0.69	0.65	0.66	0.47	0.01	0.01	0.01	1.46	1.43	1.43	0.63	0.63	0.62
RMS of Random Error σ (mm)	1.00	1.00	1.05	0.66	0.65	0.70	0.74	0.73	0.78	0.76	0.78	0.86	0.42	0.42	0.43	0.01	0.01	0.01	0.78	0.77	0.77	0.63	0.62	0.64
Oropharynx																								
Group systematic error M (mm)	0.44	0.44	0.50	−0.27	−0.09	−0.26	−0.25	−0.22	−0.30	1.62	1.55	1.59	0.10	0.06	0.15	0.00	0.00	0.00	0.07	0.04	0.09	1.35	1.28	1.19
SD of systematic error Σ (mm)	1.01	0.96	1.05	0.68	0.65	0.49	0.75	0.76	0.81	0.70	0.69	0.72	0.59	0.56	0.40	0.01	0.01	0.01	1.36	1.28	1.29	0.62	0.56	0.62
RMS of random error σ (mm)	0.99	0.99	1.03	0.53	0.49	0.44	0.63	0.60	0.63	0.70	0.72	0.78	0.46	0.44	0.35	0.01	0.01	0.01	0.73	0.71	0.70	0.61	0.59	0.58

Table 3 (*continued*)

Table 3 (*continued*)

Volumes-of-interest	3D translation												3D rotation									
	LR			AP			SI			3D			Roll			Pitch			Yaw			3D		
	HQI	p-LQI	t-LQI	HQI	p-LQI	t-LQI	HQI	p-LQI	t-LQI	HQI	p-LQI	t-LQI	HQI	p-LQI	t-LQI	HQI	p-LQI	t-LQI	HQI	p-LQI	t-LQI	HQI	p-LQI	t-LQI
Hypopharynx																								
Group systematic error M (mm)	0.40	0.36	0.41	0.06	0.16	−0.01	−0.46	−0.38	−0.33	1.61	1.54	1.51	0.32	0.20	0.26	0.00	0.00	0.00	−0.08	−0.13	−0.04	0.97	0.90	0.84
SD of systematic error Σ (mm)	1.07	1.05	1.09	0.54	0.51	0.38	0.09	0.12	0.54	0.69	0.67	0.69	0.16	0.16	0.07	0.01	0.01	0.01	0.93	0.86	0.85	0.33	0.38	0.38
RMS of random error σ (mm)	1.00	1.00	0.99	0.71	0.70	0.57	0.86	0.87	0.74	0.81	0.85	0.81	0.32	0.30	0.30	0.01	0.01	0.01	0.56	0.55	0.52	0.45	0.42	0.41

induced artifacts and geometric distortion. These are the major reasons that we selected 3D T1w SPACE for positioning MRI acquisition, although some gradient echo sequences might be able to obtain shorter scan time. In terms of scan time, positioning MRI acquisition should be as short as possible to minimize the intra-scan positional change. In addition, a scan time shorter than the commonly used on-board imaging in IGRT would be advantageous to increase the MRgRT workflow efficiency (5). This is also the reason that we set the pre-defined aim of 90 s for MR-based position verification by referring to other on-board 3D-CT position verification time. On the other hand, the scan time for MRI-based position verification should be as long as possible to pursuit better image quality in order to facilitate soft-tissue based position verification and meanwhile ensure registration accuracy. By taking the advantage of superior soft tissue contrast of MRI, position verification based on the soft tissue registration, e.g., directly tumor registration, rather than the bony structure surrogates for registration, should be a unique feature and advantage of MRgRT in the precise RT. As such, the soft tissue contrast of the MR images for position verification could not be much compromised even with a much shorter scan time. Finally, within the allowable short scan time, the voxel size, i.e., spatial resolution, of the MR images for position verification should not be too coarse and thus sacrifices image registration accuracy, in particular in the presence of the image artifacts associated with the acceleration techniques.

Based on the above consideration, a LQI-MRI protocol was developed for position verification based on GRAPPA accelerated 3D-T1-SPACE sequence. The scan time was 84 s, slightly shorter than the pre-defined aim of 90 s, and the voxel size was slightly larger, i.e., isotropic 1.4 mm. On one hand, the image quality of LQI-MRI inevitably deteriorated compared to that of HQI-MRI at the expense of the much shorter acquisition. On the other hand, the compromised image quality of LQI-MRI was believed still better than the commonly used on-board 3D-CT images, such as kv CBCT, mv CBCT and MVCT, in particular of soft tissue contrasts, to facilitate soft-tissue based overall or regional position verification. It is worth noting that an even shorter scan time might be achievable for MR-based position verification by choosing different sequence, further reducing spatial resolution, applying higher acceleration factors as well as combining with other advanced fast imaging techniques such as compressed sensing (31). Further studies and rigorous validations are warranted.

We rigorously assessed the influence of image quality reduction, in particular of low spatial resolution and parallel imaging related artifacts, on the accuracy of image registration to high quality planning MRI using both retrospectively reconstructed pseudo-LQI-MRI and prospectively acquired true-LQI-MRI. As mentioned above, the major purpose of this pseudo-LQI-MRI was to ensure its identical positioning to that in the HQI-MRI but with more pronounced acceleration artifacts. Therefore, the positional shift difference calculated from pseudo-LQI-to-reference registration and HQI-to-reference registration could completely avoid the bias and uncertainty introduced by the possible intra-scan positional change, and only resulted from the image quality reduction itself. Although pseudo- and true-LQI-MRI had the same nominal spatial-resolution, reconstruction algorithm, and acceleration factor, their image quality in terms of SNR and artifact appearance could still be markedly different. The visual assessment indicated that pseudo-LQI-MRI had generally poorer image quality and more severe GRAPPA artifact than true-LQI-MRI. Therefore, pseudo-LQI-to-reference registration might unlikely underestimate the image registration error and uncertainty due to the lower spatial resolution and acceleration artifacts. No matter pseudo- or true-LQI images were used for registration, the calculated positional errors were mostly highly consistent, even in the possible presence of intra-scan positional change for true-LQI images. These results suggested that a highly accelerated 3D MRI could be used for head and neck positional verification with high workflow efficiency but without compromising accuracy.

In our study, rigid registration of sub-regions showed that local positional error was often larger than the overall positional error, especially in LR and AP directions. As such, if position verification and correction were conducted based on the global image registration, there might still be residual sub-regional positional errors. These observations indicate the potential need of sub-regional or target based positional verification and correction in MRgRT to further increase the positional accuracy.

The implementation of MRI-based position verification for off-line and on-line MRgRT can be substantially different. For the on-line MRgRT, such as MR-LINAC, the derived positional shift from image registration is used to shift the treatment plan, in other word, to virtually shift the patient since the patient couch on the MR-LINAC is only movable along the longitudinal (SI) direction (32). With the capability of on-line MRI imaging, the patient positional scan could be conducted multiple times before, during and after the fractional treatment for different purposes. In contrast, the positional-MRI scan should be conducted on an MR-sim directly prior to the treatment for the off-line MRgRT. After that, the patient has to be physically transferred in their setup position to the treatment unit in the time as short as possible. The patient position information obtained by the positional-MRI scan also needs to be transferred to the treatment unit for registration with the planning images. It has been preliminarily verified that the patient position under immobilization would not much changed during a short transfer (24). Therefore, the on-board X-ray imaging procedure could potentially be skipped, if no correction is needed. If a substantial positional shift is found via registering positional MRI to the planning images, a positional correction will be triggered and conducted directly on the treatment unit couch in 3 degrees-of-freedom to compensate for translational shift or in 6 degrees-of-freedom to compensate for both translational and rotational shifts. Without the on-line MRI capability, the patient position checking after that has to rely on the on-board X-ray imaging modality if deemed necessary.

This study has some limitations. First, this study only recruited a small sample size of healthy volunteers, which might limit the statistical power of the analysis. More importantly, the influence of patient weight loss, tumor shrink, and tissue deformations occur during the multi-fraction treatment on MR-based position verification could not be assessed (33-35). Second, the fast MRI scan for position verification in this study was achieved mainly by high acceleration factor and spatial resolution reduction. Alternative MRI-based positional scan protocols could be implemented by using different sequences, image contrasts, and other acceleration techniques. They could not be all included and assessed in a single study so should be further investigated. The duration of the positional-MRI scan might be further reduced without compromising the accuracy of positional shift calculation. Recently, we have reduced the positioning MRI scan time of 3D T1w SPACE to 53 s and its impact on the positional verification is under investigation. Third, this study only involved the MR-MR image registration with the similar image contrast but different spatial resolution. Since planning-CT is still the clinical standard for radiotherapy treatment planning and X-ray-based on-board imaging is still the mainstream of image guidance, multi-modality co-registration of positional-MRI with other images has to be further studied (36).

The residual MRI geometric distortion (30,37,38) even after applying geometric distortion correction and its influence on position verification, in particular for multi-modality co-registration, need to be further carefully investigated. Future research work is warranted to further validate and verify the value of the proposed accelerated 3D MRI for both on- and off-line MRI position verification. On the newly introduced 1.5 T MR-LINAC, most of the current pre-set imaging protocols are based on 3D pulse sequences other than T1w SPACE with longer acquisition time than the proposed one in this study. They are usually not acquired but rather reconstructed in isotropic voxel size. The implementation and evaluation of the proposed positioning MRI on 1.5 T MR-LINAC is under way. For off-line MRI positioning verification, the positional variation introduced by the patient transfer procedure is still concerned on real patients, although our preliminary study indicated that the overall position shift of healthy volunteers after transportation measured by rigid registrations were very small and acceptable (39). The related study is to be conducted in the near future.

Acknowledgments

None.

Footnote

Conflicts of Interest: The authors have no conflicts of interest to declare.

Ethical Statement: The study was approved by institutional research ethics committee (RC-2015-08) and written informed consent was obtained from all patients.

References

1. Verellen D, De Ridder M, Storme G. A (short) history of image-guided radiotherapy. Radiother Oncol 2008;86:4-13.
2. Dawson LA, Jaffray DA. Advances in image-guided radiation therapy. J Clin Oncol 2007;25:938-46.
3. Qi XS, Hu AY, Lee SP, Lee P, DeMarco J, Li XA, Steinberg ML, Kupelian P, Low D. Assessment of interfraction patient setup for head-and-neck cancer intensity modulated radiation therapy using multiple computed tomography-based image guidance. Int J Radiat Oncol Biol Phys 2013;86:432-9.
4. Dionisi F, Palazzi MF, Bracco F, Brambilla MG, Carbonini C, Asnaghi DD, Monti AF, Torresin A. Set-up errors and planning target volume margins in head and neck cancer radiotherapy: a clinical study of image guidance with on-line cone-beam computed tomography. Int J Clin Oncol 2013;18:418-27.
5. Korreman S, Rasch C, McNair H, Verellen D, Oelfke U, Maingon P, Mijnheer B, Khoo V. The European Society of Therapeutic Radiology and Oncology-European Institute of Radiotherapy (ESTRO-EIR) report on 3D CT-based in-room image guidance systems: a practical and technical review and guide. Radiother Oncol 2010;94:129-44.
6. Bissonnette JP, Purdie TG, Higgins JA, Li W, Bezjak A. Cone-beam computed tomographic image guidance for lung cancer radiation therapy. Int J Radiat Oncol Biol Phys 2009;73:927-34.
7. Den RB, Doemer A, Kubicek G, Bednarz G, Galvin JM, Keane WM, Xiao Y, Machtay M. Daily image guidance with cone-beam computed tomography for head-and-neck cancer intensity-modulated radiotherapy: a prospective study. Int J Radiat Oncol Biol Phys 2010;76:1353-9.
8. Langen KM, Zhang Y, Andrews RD, Hurley ME, Meeks SL, Poole DO, Willoughby TR, Kupelian PA. Initial experience with megavoltage (MV) CT guidance for daily prostate alignments. Int J Radiat Oncol Biol Phys 2005;62:1517-24.
9. Kilby W, Dooley JR, Kuduvalli G, Sayeh S, Maurer CR, Jr. The CyberKnife Robotic Radiosurgery System in 2010. Technol Cancer Res Treat 2010;9:433-52.
10. Henke LE, Contreras JA, Green OL, Cai B, Kim H, Roach MC, Olsen JR, Fischer-Valuck B, Mullen DF, Kashani R, Thomas MA, Huang J, Zoberi I, Yang D, Rodriguez V, Bradley JD, Robinson CG, Parikh P, Mutic S, Michalski J. Magnetic Resonance Image-Guided Radiotherapy (MRIgRT): A 4.5-Year Clinical Experience. Clin Oncol (R Coll Radiol) 2018;30:720-7.
11. El-Bared N, Portelance L, Spieler BO, Kwon D, Padgett KR, Brown KM, Mellon EA. Dosimetric Benefits and Practical Pitfalls of Daily Online Adaptive MRI-Guided Stereotactic Radiotherapy for Pancreatic Cancer. Pract Radiat Oncol 2019;9:e46-54.
12. Chen AM, Hsu S, Lamb J, Yang Y, Agazaryan N, Steinberg ML, Low DA, Cao M. MRI-guided radiotherapy for head and neck cancer: initial clinical experience. Clin Transl Oncol 2018;20:160-8.
13. Pollard JM, Wen Z, Sadagopan R, Wang J, Ibbott GS. The future of image-guided radiotherapy will be MR guided. Br J Radiol 2017;90:20160667.
14. Menten MJ, Wetscherek A, Fast MF. MRI-guided lung

SBRT: Present and future developments. Phys Med 2017;44:139-49.
15. Cao Y, Tseng CL, Balter JM, Teng F, Parmar HA, Sahgal A. MR-guided radiation therapy: transformative technology and its role in the central nervous system. Neuro Oncol 2017;19:ii16-29.
16. Lagendijk JJ, van Vulpen M, Raaymakers BW. The development of the MRI linac system for online MRI-guided radiotherapy: a clinical update. J Intern Med 2016;280:203-8.
17. Yuan J, Lo G, King AD. Functional magnetic resonance imaging techniques and their development for radiation therapy planning and monitoring in the head and neck cancers. Quant Imaging Med Surg 2016;6:430-48.
18. Bostel T, Nicolay NH, Grossmann JG, Mohr A, Delorme S, Echner G, Haring P, Debus J, Sterzing F. MR-guidance--a clinical study to evaluate a shuttle- based MR-linac connection to provide MR-guided radiotherapy. Radiat Oncol 2014;9:12.
19. Raaymakers BW, Lagendijk JJ, Overweg J, Kok JG, Raaijmakers AJ, Kerkhof EM, van der Put RW, Meijsing I, Crijns SP, Benedosso F, van Vulpen M, de Graaff CH, Allen J, Brown KJ. Integrating a 1.5 T MRI scanner with a 6 MV accelerator: proof of concept. Phys Med Biol 2009;54:N229-37.
20. Lagendijk JJ, Raaymakers BW, Van den Berg CA, Moerland MA, Philippens ME, van Vulpen M. MR guidance in radiotherapy. Phys Med Biol 2014;59:R349-69.
21. Zhou Y, Yuan J, Wong OL, Fung WW, Cheng KF, Cheung KY, Yu SK. Assessment of positional reproducibility in the head and neck on a 1.5-T MR simulator for an offline MR-guided radiotherapy solution. Quant Imaging Med Surg 2018;8:925-35.
22. Lagendijk JJ, Raaymakers BW, van Vulpen M. The magnetic resonance imaging-linac system. Semin Radiat Oncol 2014;24:207-9.
23. Mutic S, Dempsey JF. The ViewRay system: magnetic resonance-guided and controlled radiotherapy. Semin Radiat Oncol 2014;24:196-9.
24. Bostel T, Pfaffenberger A, Delorme S, Dreher C, Echner G, Haering P, Lang C, Splinter M, Laun F, Muller M, Jakel O, Debus J, Huber PE, Sterzing F, Nicolay NH. Prospective feasibility analysis of a novel off-line approach for MR-guided radiotherapy. Strahlenther Onkol 2018;194:425-34.
25. Paulson ES, Erickson B, Schultz C, Allen Li X. Comprehensive MRI simulation methodology using a dedicated MRI scanner in radiation oncology for external beam radiation treatment planning. Med Phys 2015;42:28-39.
26. Devic S. MRI simulation for radiotherapy treatment planning. Med Phys 2012;39:6701-11.
27. Griswold MA, Jakob PM, Heidemann RM, Nittka M, Jellus V, Wang J, Kiefer B, Haase A. Generalized autocalibrating partially parallel acquisitions (GRAPPA). Magn Reson Med 2002;47:1202-10.
28. Fedorov A, Beichel R, Kalpathy-Cramer J, Finet J, Fillion-Robin JC, Pujol S, Bauer C, Jennings D, Fennessy F, Sonka M, Buatti J, Aylward S, Miller JV, Pieper S, Kikinis R. 3D Slicer as an image computing platform for the Quantitative Imaging Network. Magn Reson Imaging 2012;30:1323-41.
29. van Herk M. Errors and margins in radiotherapy. Semin Radiat Oncol 2004;14:52-64.
30. Walker A, Liney G, Metcalfe P, Holloway L. MRI distortion: considerations for MRI based radiotherapy treatment planning. Australas Phys Eng Sci Med 2014;37:103-13.
31. Lustig M, Donoho D, Pauly JM. Sparse MRI: The application of compressed sensing for rapid MR imaging. Magn Reson Med 2007;58:1182-95.
32. Bol GH, Lagendijk JJ, Raaymakers BW. Virtual couch shift (VCS): accounting for patient translation and rotation by online IMRT re-optimization. Phys Med Biol 2013;58:2989-3000.
33. Wong KH, Panek R, Bhide SA, Nutting CM, Harrington KJ, Newbold KL. The emerging potential of magnetic resonance imaging in personalizing radiotherapy for head and neck cancer: an oncologist's perspective. Br J Radiol 2017;90:20160768.
34. Yu Y, Michaud AL, Sreeraman R, Liu T, Purdy JA, Chen AM. Comparison of daily versus nondaily image-guided radiotherapy protocols for patients treated with intensity-modulated radiotherapy for head and neck cancer. Head Neck 2014;36:992-7.
35. Polat B, Wilbert J, Baier K, Flentje M, Guckenberger M. Nonrigid patient setup errors in the head-and-neck region. Strahlenther Onkol 2007;183:506-11.
36. Daisne JF, Sibomana M, Bol A, Cosnard G, Lonneux M, Gregoire V. Evaluation of a multimodality image (CT, MRI and PET) coregistration procedure on phantom and head and neck cancer patients: accuracy, reproducibility and consistency. Radiother Oncol 2003;69:237-45.
37. Weygand J, Fuller CD, Ibbott GS, Mohamed AS, Ding Y, Yang J, Hwang KP, Wang J. Spatial Precision in Magnetic Resonance Imaging-Guided Radiation Therapy: The Role

of Geometric Distortion. Int J Radiat Oncol Biol Phys 2016;95:1304-16.
38. Baldwin LN, Wachowicz K, Thomas SD, Rivest R, Fallone BG. Characterization, prediction, and correction of geometric distortion in 3 T MR images. Med Phys 2007;34:388-99.
39. Cheng KF, Fok PH, Chiu G, Mui WL. Position Accuracy of Using Patient Positioning and Transfer System With Head and Neck Immobilization. Int J Radiat Oncol Biol Phys 2017;99:E647.

Cite this article as: Zhou Y, Wong OL, Cheung KY, Yu SK, Yuan J. A pilot study of highly accelerated 3D MRI in the head and neck position verification for MR-guided radiotherapy. Quant Imaging Med Surg 2019;9(7):1255-1269. doi: 10.21037/qims.2019.06.18

